

# The Calibration of the UVIT Detectors for the ASTROSAT Observatory

Denis Leahy<sup>1</sup>, J. Postma<sup>1</sup>, J. B. Hutchings<sup>2</sup> and S. N. Tandon<sup>3,4</sup>

<sup>1</sup>Dept. of Physics and Astronomy, University of Calgary, Calgary, AB, T2N 1N4, Canada  
email: [leahy@ucalgary.ca](mailto:leahy@ucalgary.ca)

<sup>2</sup>Herzberg Institute of Astrophysics, 5071 West Saanich Road, Victoria, BC V9E 2E7, Canada

<sup>3</sup>Inter-University Center for Astronomy and Astrophysics, Pune, India

<sup>4</sup>Indian Institute of Astrophysics, Koramangala II Block, Bangalore-560034, India

**Abstract.** The UVIT ultraviolet and visual band detectors and electronics for the ASTROSAT observatory were calibrated in the vacuum laboratory at the University of Calgary. This work was supported by the Canadian Space Agency and carried out prior to integration with the UVIT optical assembly and the ASTROSAT spacecraft. The multiband (X-ray, ultraviolet and optical) ASTROSAT observatory was successfully launched by the Indian Space Research Organization on Sept. 28, 2015, with subsequent in-orbit verification and ongoing calibration activities. Here we discuss the current issues of calibrating the UVIT data, such as distortion corrections, and how the laboratory data is being used to address these issues.

**Keywords.** instrumentation: detectors, techniques: image processing, techniques: photometric

---

## 1. Introduction

AstroSat is a multiwavelength space observatory of the Indian Space Research Organisation (ISRO), with contributions by the Canadian Space Agency and the University of Leicester. The satellite contains three pointed X-ray instruments and two ultraviolet (UV) and optical telescopes, all with fields of view that are aligned. An additional instrument is the all-sky X-ray scanning monitor. The full observatory details and capability are described in the ISRO World Wide Web site. The observatory constitutes a multiwavelength capability that allows simultaneous monitoring of targets from optical/UV wavelengths to 100 keV with high timing precision. The twin UV-optical telescopes (UVITs) have a 38 cm aperture and field of view of 28 arcmin, with 1.3 arcsec spatial resolution. One telescope covers the far UV (FUV) and the other covers the near UV (NUV) and blue optical bands using a beam splitter.

The ground calibration of UVIT detectors was discussed in Postma *et al.* (2011). Custom software was developed to implement calibration procedures with data from the instrument in science operation mode. A description of the software package is given in Postma *et al.* (2017). The scientific performance of the UVIT instrument and its space calibration is discussed in Subramaniam *et al.* (2017) and Tandon *et al.* (2017). Some of the first scientific results with UVIT are described in e.g. George *et al.* (2018) and Leahy *et al.* (2018).

Here we describe briefly the calibrations and corrections that have to be applied to the raw centroid data from the UVIT telescopes. These are required to produce images which are useful for science analysis.

## 2. Discussion

Fig. 1 shows the flat field for the NUV which was measured by on-ground calibrations with an integrating sphere. The FUV channel flat field was similarly measured and is

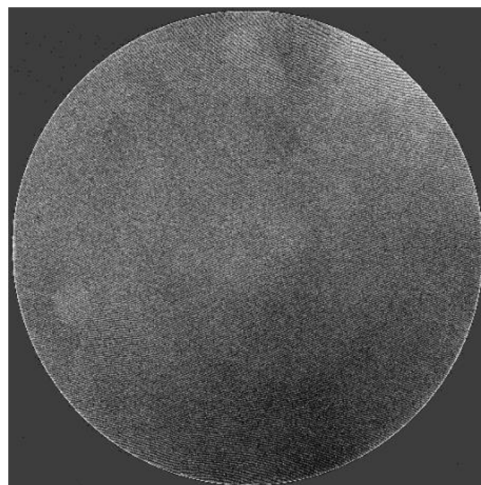


**Figure 1.** NUV flat-field image.

not shown, but is similar in quality to the NUV image figure. All centroids are thus given a weight corresponding to their position at which they were detected in the field. That is, a centroid nominally represents a unit detection of a photon event. However, at nominal high operating voltage for the detector there is a small variation in probability (10% across the field) that a photon will be detected when considering a large number of possible detections. Thus, the inverse of the detected flat field at a given location provides the weight of the centroid in that location: if the normalized flat field has a value of 0.9 where the photon falls, then relative to the normal that region is under-detecting and so a photon in that region is given a weight of  $1/0.9$ . Because a centroid is a set of coordinates, the centroid list or table of photon event detection coordinates has a corresponding table list of coordinate weights. It is important to record the photon event weights at the initial ingestion of the data because later corrections for drift must move the photon event coordinates from their detected positions during the drift movements to a mean drift-corrected frame of coordinates which then no longer correspond to the detection coordinates.

The measurement of the flat field also provides for characterization of the fixed-pattern-noise (FPN) or centroiding bias introduced into the determination of the photon event centroids. The photon events are relatively under-sampled on the CMOS detector, having a FWHM (full width half maximum) of only approximately  $1.3 \pm 0.3$  pixels. Sub-pixel resolution of photon event centroids is a design requirement of this system in order to achieve the desired 1" resolution, corresponding to  $1/3$  of a pixel of the CMOS chip. The photon event centroids are determined by a simple weighted mean of values and positions of the photon pulse over a 3x3 pixel kernel which captures  $\approx 95\%$  of the photon event energy, and are recorded by the detector system at 1/32 pixel resolution. A 5x5 kernel was also explored in ground calibrations since this would capture the remaining 5% of signal of the photon event pulse, but it was found that the read noise in the outer 16 pixels prevented any improvement in the centroid determination. Thus, a weighted mean of an under-sampled approximately Gaussian signal provides centroids which have a preferential bias towards symmetry, that is, a centroid with a sub-pixel decimal value which pulls to zero. A truly symmetric photon event pulse on the CMOS results in a centroid with a decimal place of 0, while an asymmetric photon event pulse will have a non-zero decimal value but which is systematically biased towards zero. This can be seen in the left panel of Figure 2. This FPN bias can be measured and then corrected for by

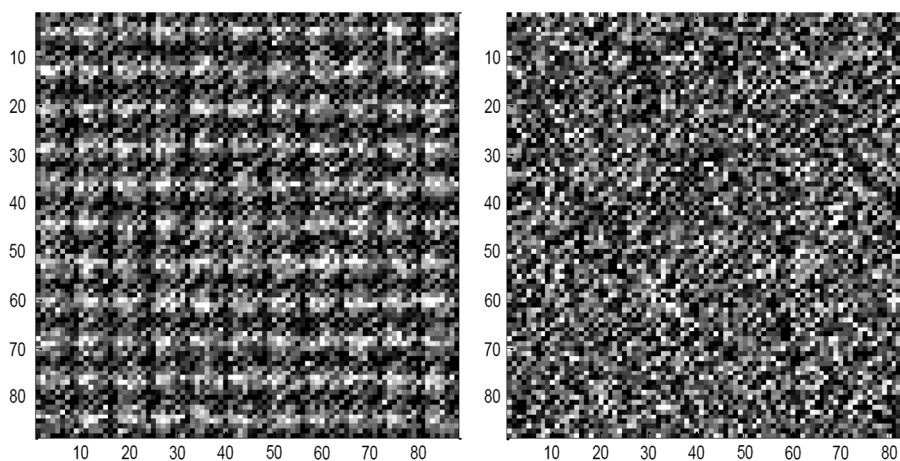


**Figure 2.** Closeup of a small region of the NUV image. Left panel: flat field image prior to fixed-pattern noise (FPN) correction. The FPN of the detector is seen in the image before correction. Right Panel: flat field image after the FPN correction.

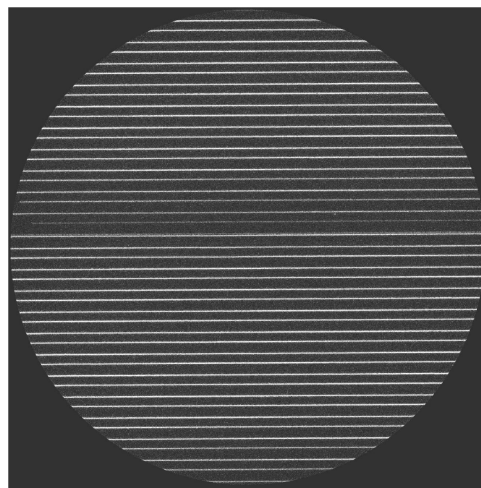


**Figure 3.** NUV image taken in laboratory with scanning of pinhole image for the purpose of distortion corrections. When examined in detail, the straight lines are imaged as curved lines. The distortion correction restores the lines to be straight.

determining the cumulative probability distribution of the decimal-places of all centroids detected from a flat field source, since a flat field will have no sub-pixel preferentiality. The FPN corrected flat field image can be seen on the right panel of Fig. 2.

For astrometric accuracy the fields must be corrected for distortions introduced by the fiber-optic taper (and other possible contributions). During ground-calibrations the detectors were continuously run while being scanned in either axis across their window with a micrometer stage and a multi-pinhole mask with rear-illumination, the result for the horizontal axis shown in Fig. 3. Measured at 1/8th subpixel resolution, after being corrected for the FPN, it is found that the scan lines are not straight lines but have structure resembling a quadratic curve exceeding several CMOS pixels variation from a straight line. Given that the detected lines were supposed to be straight lines, then the residuals of the detected line centroid coordinates from a fitted straight line provides the distortion across the field, and this is performed for each line and in both horizontal and

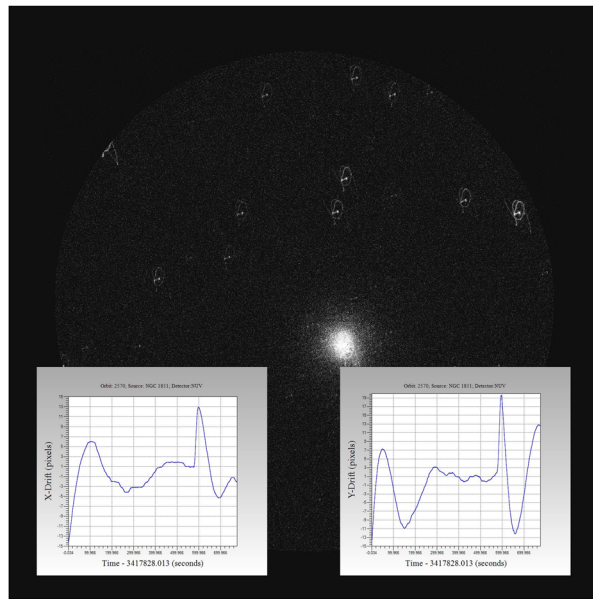


**Figure 4.** In-orbit NUV image of a field containing foreground stars and a globular cluster (below and right of centre). Star images are clearly trailed because of spacecraft pointing errors. The globular cluster image is also trailed which results in severe smearing.

vertical scan axes. The in-flight astrometry is thus improved to an accuracy approaching 1 arc second. Additional calibrations were done by imaging a 2-D grid of pin-holes. For details please see [Girish \*et al.\* \(2017\)](#).

For in-flight imaging of science targets, the ASTROSAT satellite is flown with an induced sinusoidal drift or dithering of nominal rate 1" per second and amplitude 80" in orthogonal axes. The purpose of this is to spread charge depletion of the microchannel plates inside the detectors evenly about their detector face, on average. In addition, there are random drifts up to  $\sim 2''/\text{s}$ . The visible (VIS) channel is used for tracking the drift given that VIS-bright point sources (stars) are expected in any given observation, and the cadence of the VIS imaging for tracking is 1 Hz. The science data centroids in FUV and NUV channels are however gathered at approximately 30 Hz, and so the drift series determined from VIS at 1 Hz must be interpolated, typically with a simple cubic spline, to the times of the FUV and NUV centroids. A drift series can be seen in Fig. 4, along with the trailed-star image produced before drift-correction is applied, and Fig. 5 demonstrates the final science image after all corrections.

### 3. Summary

We have discussed briefly the various corrections to UVIT images required to put them in a form which is useful for imaging and photometry for science analysis. Corrections for flat-fielding, distortions and spacecraft pointing errors are essential to restore the images to the design spatial resolution, and to allow photometry, positions and shapes of astronomical images to be accurately determined in the NUV and FUV bands.

The Indian Space Science Data Centre (ISSDC) archives the final astronomer ready UVIT products (sky images in UV, exposure, etc) generated by the Payload Operation Centre (POC) at the Indian Institute of Astrophysics (IIA), using the UVIT Level-2 Pipeline developed by ISRO and the UVIT instrument team (<http://uvit.iap.res.in/Downloads>).



**Figure 5.** NUV image of the same field containing foreground stars and a globular cluster (below and right of centre), after correction for trailing. The star images are now pointlike and the globular cluster is seen clearly.

### Acknowledgement

This work was supported by the Canadian Space Agency.

### References

- George, K., Poggianti, B. M., Gullieuszik, M., *et al.* 2018, *MNRAS*, 479, 4126  
Leahy, D., Bianchi, L. & Postma, J. 2018, *ApJ*, submitted  
Girish, V., Tandon, S. N., Sriram, S., Kumar, A., & Postma, J 2017, *Experimental Astronomy*, 143, 59  
Postma, J., Hutchings, J. B., & Leahy, D. 2011, *PASP*, 123, 833  
Postma, J. E., & Leahy, D. 2017, *PASP*, 129, 115002  
Subramaniam, A., Sindhu, N., Tandon, S. N., *et al.* 2017, *ApJ*, 833, L27  
Tandon, S. N., Subramaniam, A., Girish, V., *et al.* 2017, *AJ*, 154, 128